Journal of the European Ceramic Society 23 (2003) 519–525

www.elsevier.com/locate/jeurceramsoc

Room temperature electrochemical growth of polycrystalline $BaMoO_4$ films

Chang-Tai Xia[1], V.M. Fuenzalida*

Departamento de Física FCFM, Universidad de Chile, Casilla 487-3, Santiago 6511226, Chile

Received 29 May 2001; accepted 5 May 2002

Abstract

The pH-concentration diagram for the formation of barium molybdate films on a metallic molybdenum substrate in a barium hydroxide aqueous solution has been experimentally studied. Due to the relatively large solubility of the molybdate, the estimation of film thickness from the weight gain was corrected by considering the substrate dissolution. The molybdenum substrates had a preferential [100] crystallographic orientation, but the films exhibited no preferential orientation. It is suggested that the film grows through a dissolution-precipitation mechanism and that nucleation begins only after the solution is locally saturated with barium molybdate. Irregular intergrowth is frequent due to the high crystal growth rate. XPS measurements on samples that appeared completely coated under SEM examination exhibited only the peaks corresponding to barium molybdate. On the other hand, the substrates that appeared partially coated under SEM, when examinated by XPS exhibited the superposition of spectra of the molybdate and of the uncoated molybdenum substrate. This allows the study of the degree of coating as a function of the solution concentration and pH.

Keywords: $BaMoO_4$; Films; Growth processes; Microstructure-final

1. Introduction

The preparation of functional ceramic coatings and powders using electrochemical methods is a relatively new technology that takes advantage of the large amount of work carried out on metallic corrosion and electrodeposition.[1–19] The advantages of electrochemical coating techniques over more conventional techniques have been summarized by Switzer.[1] The thickness and morphology of the ceramic films can be controlled by the electrochemical parameters and relatively uniform deposits can be obtained on complex shapes. With accurate control of the applied potential, Switzer has already shown that nanoscale superlattices can be deposited at room temperature.[2,3] Equally attractive is the fact that the equipment is inexpensive and the technique has the potential to synthesize crystalline films near room temperature in large-scale operations.[4]

As for the anodic method, synthesis of several types of oxide films and powders have been reported, such as thallium oxide films on silicon substrates,[1,5] $BaTiO_3$ and $SrTiO_3$ films on titanium substrates,[6–10] $BaTiO_3$ powders,[11] and ZrO_2 films on zirconium substrates.[4]

Recently, Cho et al.[12–19] reported the room temperature deposition of films of luminescent materials such as $CaWO_4$, $SrWO_4$, and $Ca_{(1-x)}Sr_xWO_4$ on tungsten substrates, and $CaMoO_4$, $SrMoO_4$, and $BaMoO_4$ films on molybdenum foils. These materials belong to the scheelite group[20] and produce blue or green luminescence. Single crystals of these materials have been studied as hosts for lanthanide activated lasers.[21] In the present paper we report on the growth of $BaMoO_4$ films, particularly on the effect of pH, Ba^{2+} ion concentration, and treatment time.

2. Experiment

A Teflon container was used as the reaction vessel in all experiments to minimize contamination. All surfaces in contact with the electrolyte solution were made of

* Corresponding author. Tel.: +56-22-678-4392; fax: +56-22-696-7359.

E-mail address: vfuenzal@cec.uchile.cl (V.M. Fuenzalida).

[1] Present address: Toyota Central R&D Labs., Inc., Nagakote, Aichi, 480-1192, Japan.

0955-2219/02/$ - see front matter
PII: S0955-2219(02)00149-8

Teflon, except for the platinum cathode and the molybdenum anode. The electrodes were parallel, separated by 28 mm and were suspended from platinum wires and immersed in the electrolyte. The molybdenum working electrodes were cut from a 0.1 mm thick molybdenum foil (Alfa®, 99.95%) into 20 mm×20 mm plates. They were degreased in acetone, chemically etched by 6 N HCl for 24 h, washed with deionized water in an ultrasonic bath, and finally dried and weighed. Barium hydroxide solutions were prepared from high purity $Ba(OH)_2{\cdot}8H_2O$ (Sr < 0.024%, Solvay-Sabed, Italy). The deionized water was preheated to remove dissolved CO_2 and purged with N_2 gas for 30 min. pH values were adjusted with 12 N KOH and 12 N HCl. All the experiments were performed at room temperature (22–23 °C) with a current density of 1 mA/cm^2 generated by a commercial potentiostat/galvanostat power source (Model 363, Princeton Applied Research Co., USA).

Following the electrochemical treatments, the molybdenum electrodes were washed with deionized water, dried and weighted. The products were characterized by X-ray diffraction (XRD) using CuK_α radiation at 40 kV and 30 mA at a scan rate of 1.2 2θ/min (Siemens D5000 system). The 2θ range was from 20 to 80°. Scanning electron microscopy (SEM) was used to characterize the grain size, morphology, and microstructure of the films (JSM-25SII and JSM-5410, JEOL, Tokyo, Japan). An energy-dispersive x-ray spectrometer (EDS) attached to a SEM was used to map the elemental distribution of the film surfaces (JSM-6400K SEM with an Oxford EDS). Further characterization was performed by X-ray photoelectron spectrometry (XPS) assisted by argon ion sputtering (Physical Electronics 1257 system).

3. Results and discussion

3.1. Formation diagram

Fig. 1 shows the pH-concentration diagram of the $BaMoO_4$ films prepared under a current density of 1 mA/cm^2 under galvanostatic conditions by the electrochemical method. The experiments were carried out at different concentrations of $Ba(OH)_2$ aqueous solutions and at different pH values. The formation of $BaMoO_4$ crystals was confirmed by XRD, and the crystallytes were observed by optical microscopy and SEM. The threshold for growth–no growth of $BaMoO_4$ crystals for a given $Ba(OH)_2$ solution is shown in the figure.

3.2. Thickness

Along with the growth of the film on the metal substrates, the weight of the substrates changed, usually increasing. This increase in weight was used to estimate the film thickness as was performed in samples of

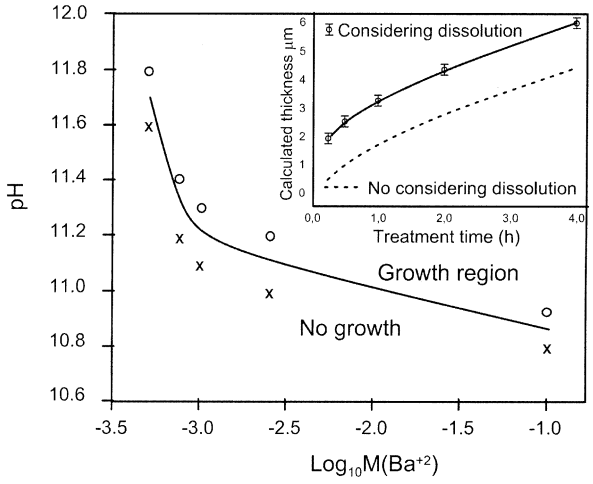

Fig. 1. pH-concentration diagram of $BaMoO_4$ at 295 K under 1 mA/cm^2. Inset: calculated film thickness vs. treatment time.

$BaTiO_3$[9] and $BaZrO_3$,[22] assuming that no dissolution of the film or the substrate took place. In fact, a weight decrease was observed in some cases, attributed to substrate dissolution. The solubility of $BaMoO_4$ at 23 °C is 0.0058 g per 100 cc cold water,[23] thus the solubility product of $BaMoO_4$:

$$K_{sp(BaMoO_4)} = (0.0058/[297.27 \times 0.1])^2 = 3.8 \times 10^{-8} \quad (1)$$

Therefore the thickness t of the $BaMoO_4$ film could be calculated from the following corrected formula:

$$t = (W_o + W_s)\cdot M_{BaMoO_4}/(\rho \cdot M_{BaO_4}) \quad (2)$$

where W_o is the measured mass change, W_s is the mass loss of the substrate attributed to dissolution, M is the molecular weight of the indicated species (297.27 g/mol for $BaMoO_4$, 201.33 g/mol for BaO_4, and 95.94 g/mol for molybdenum), $\rho = 4.65$ g/cm^3 is the density of $BaMoO_4$, and $2A$ is the area of the substrate in cm^2, considering both faces.

In order to estimate W_s, we assumed that after the reaction of the solution was still a saturated solution of $BaMoO_4$, therefore the following equation should be satisfied:

$$W_s = M_{Mo}\cdot K_{sp(BaMoO_4)}/([Ba(OH)_2] - (W_o + W_s)/M_{BaMoO4}) \quad (3)$$

where $[Ba(OH)_2]$ is the initial molar concentration of $Ba(OH)_2$.

3.3. Microstructure

The inset of Fig. 1 shows the calculated thickness of the films grown in 0.01 M $Ba(OH)_2$ solution with different treatment times with and without consideration

of substrate dissolution. The film thickness considering substrate dissolution came out approximately 1.5 μm larger than those without this correction. Fig. 2 is a SEM micrograph of the cross section of the film treated for 2 h in the 0.01 M solution, and it shows that the film is not homogeneous. Its thickness ranges from 4 to 7 μm. This value is in good agreement with the calculated thickness taking into account the dissolution of the Mo substrate (4.4 μm), while the calculated thickness without this consideration amounts only to 2.9 μm.

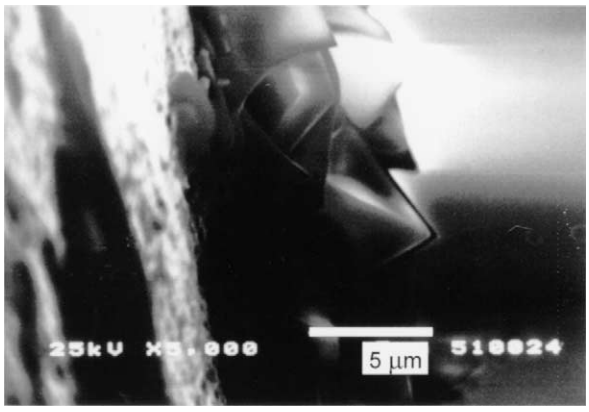

Fig. 2. SEM micrograph of the cross-section of an electrochemically prepared $BaMoO_4$ film at 1 mA/cm^2 during 2 h with a $Ba(OH)_2$ concentration of 0.01 M.

Fig. 3 shows the microstructure development of the films formed in 0.01 M $Ba(OH)_2$ solution after different electrochemical treatment times. It shows that the crystallites first formed along the lines generated by the rolling process on the foil (Fig. 3a), and exhibiting a typical tetragonal habit. We believe that the etching pits concentrate along the lines associated with the rolling direction and that they acted as nucleation centers. The crystallite size ranged from 3–7 μm (15 min) to 10–17 μm (4 h). In some cases, e.g., when the treatment was carried out in a more concentrated solution, the crystals may grow preferentially in the horizontal direction (Fig. 4) along the substrate.

3.4. Growth mechanism

The nucleation of the $BaMoO_4$ crystals initiates at surface defects along the rolling direction of the metal

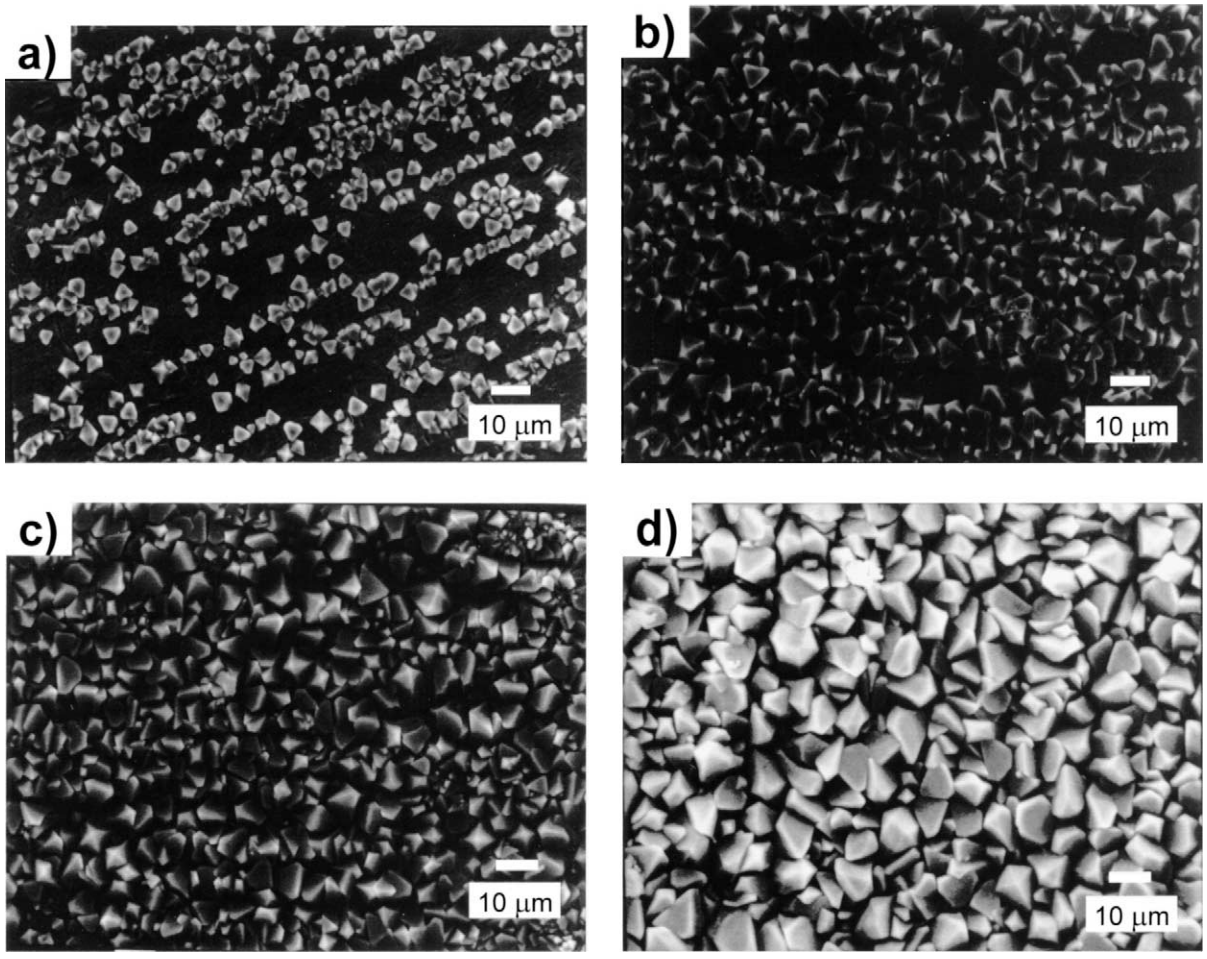

Fig. 3. SEM micrographs of the surfaces of $BaMoO_4$ films formed in 0.01 M $Ba(OH)_2$ for (a) 15 min, (b) 30 min, (c) 1 h, and (d) 4 h. The white bars represent 10 μm.

foil, as shown in the SEM micrographs in Figs. 3(a) and 5(a). A similar behavior has been observed when growing hydrothermal $BaTiO_3$ deposits on polished TiO_2 single crystals.[24] $BaMoO_4$ crystals grew in a {111} form with a dipyramidal habit. In one system twins are expected to obey a single twin law,[25] but we also observed intergrowth, even multicomponent intergrowth (''triplets'', ''quadruplets'', ''sextuplets'', etc.), and several mutual arrangements of the intergrown domains are observed in Fig. 5(a). Moreover, we are not aware of any reports of $BaMoO_4$ twins in the literature. Therefore, we suggest that the observed intergrowths are just irregular ones caused by the rapid crystal growth. A definitive answer should be given by the Kichuchi method (electron diffraction).

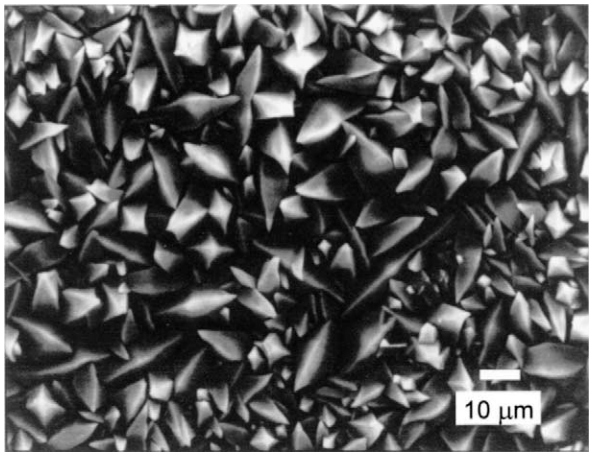

Fig. 4. SEM micrograph of the surface of a $BaMoO_4$ film formed in 0.2 M $Ba(OH)_2$ (1 h electrochemical treatment).

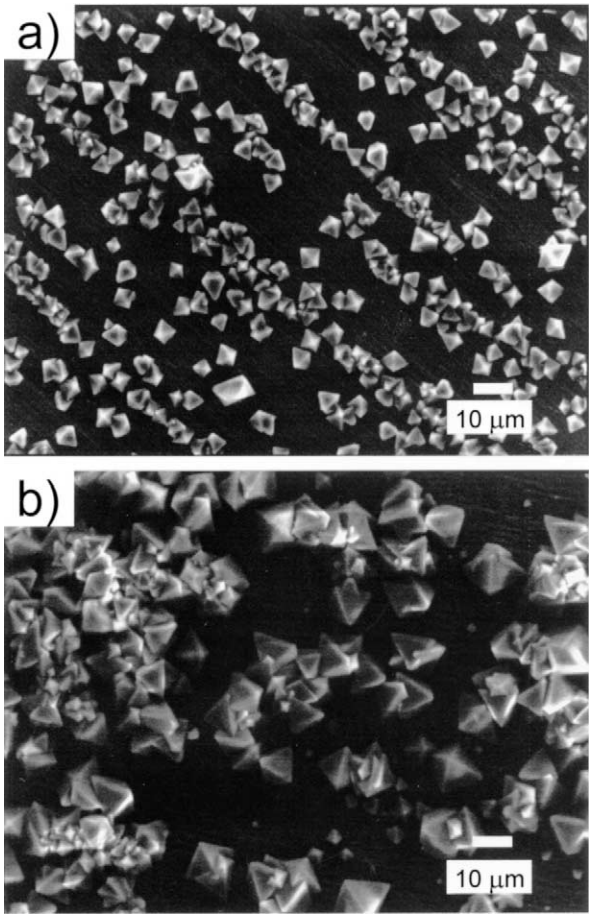

Fig. 5. SEM micrograph of the surfaces of the $BaMoO_4$ films formed in (a) 0.0025 M $Ba(OH)_2$ for 1 h and (b) 0.001 M $Ba(OH)_2$ for 2 h.

The films were well crystallized as revealed by the line broadening (full width at half maximum) FWHM measured for different XRD reflections of several samples, between 0.076 and 0.086°, while the FWHM of the standard α-SiO_2 sample provided by Siemens is 0.080°.

From the XRD results of Fig. 6, the intensity ratio between the main (110):(200):(211) reflections of the molybdenum substrate is 100:5600:1600, while the same ratio for the polycrystalline material (bars in Fig. 6) is 100:16:31.[26] We conclude that the molybdenum substrate was oriented in the [100] direction. The $BaMoO_4$ films did not show any distinct orientation [Fig. 6(b)]. The lattice parameters were refined using the UnitCell program by Holland and Redfern.[27,28] The refined lattice parameters, shown in Table 1 for a film grown in 0.01 M $Ba(OH)_2$ after a 2 h electrochemical treatment, are in good agreement with the literature.[29]

The electron probe microanalysis revealed that the films are crystalline $BaMoO_4$. Fig. 7 shows the SEM

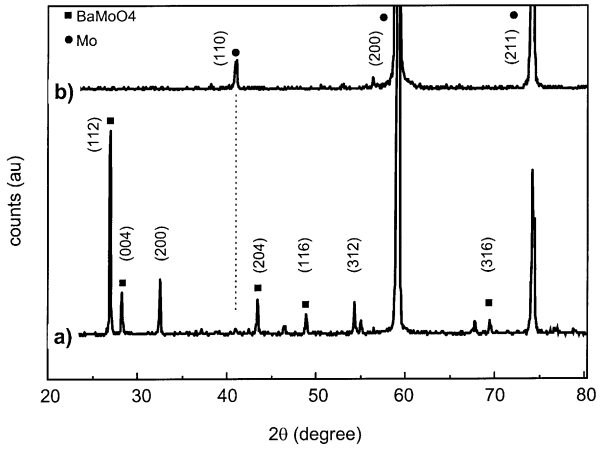

Fig. 6. X-ray diffraction patterns of (a) a $BaMoO_4$ film prepared on a molybdenum substrate in 0.01 M $Ba(OH)_2$ aqueous solution by electrochemical treatment for 30 min; (b) the untreated substrate.

Table 1
Lattice parameters for the $BaMoO_4$ film

Lattice parameters	Present work	Ref. 25
a	5.5801±0.0005[a]	5.5802
c	12.8172±0.0015[a]	12.814

[a] Standard error of the residuals.

micrograph of a sample prepared in 0.01 M $Ba(OH)_2$ for 15 min under 1 mA/cm^2 and its corresponding oxygen Kα and barium Lα1 maps. The elemental distribution analysis revealed that the molybdenum is distributed all over the film surface. Therefore, the crystallites consist of Ba, Mo and O, which should be crystalline $BaMoO_4$ as indicated by XRD. Fig. 7(b) shows the elemental distribution of barium, exhibiting maxima at the positions of the grains of the micrograph 7(a), confirming that these islands are barium-rich and correspond to the $BaMoO_4$ nuclei. The oxygen map is more diffuse, probably because the whole surface is oxidized.

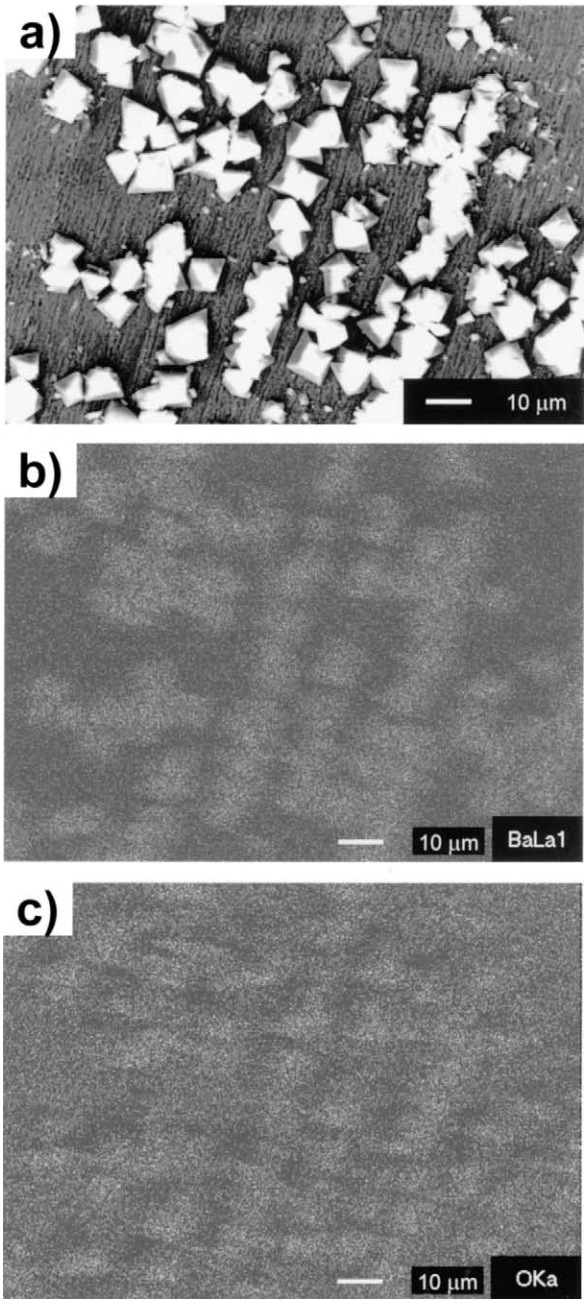

Fig. 7. (a) SEM micrograph of the surface of the $BaMoO_4$ film formed in 0.01 M $Ba(OH)_2$ for 15 min under 1 mA/cm^2, corresponding (b) oxygen Kα map and (c) barium Lα1 map.

Under the effect of the potential, molybdenum dissolves into the solution as MoO_4^{2-} ions, which should be hydrolyzed. As soon as the product of the concentrations of MoO_4^{2-} and Ba^{2+} becomes larger than the solubility product of $BaMoO_4$, $BaMoO_4$ crystals begin to nucleate at the energetically active points (i.e. etching pits). As the Mo substrate continues to dissolve, the concentration of MoO_4^{2-} increases and the crystallites grow further, with a mechanism similar to that of $BaWO_4$.[12] As growth proceeds, the surface of the substrate is almost sealed by the film, leaving only capillary channels between the crystallites, which serve as channels for further substrate dissolution.

3.5. XPS measurements

Finally, surface analysis techniques were used to provide a chemical analysis independent to the electron probe microanalysis. The samples that appeared either completely or partially coated in the SEM micrographs were examined by XPS in order to compare their surface composition. Fig. 8 shows the spectra of (a) a sample partially coated and (b) a sample completely coated, both after surface cleaning with Ar ions. Spectrum (b) was rescaled so that the intensity of the Mo3p peak of

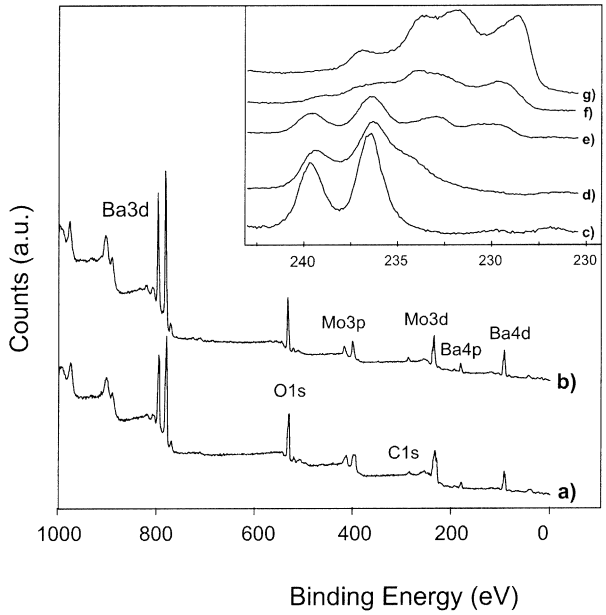

Fig. 8. XPS spectra of (a) a partially coated sample and (b) a completely coated sample after surface cleaning with Ar ions, showing a different relative amount of barium. Spectrum (b) was rescaled so that the Mo3d peak has the same intensity as in spectrum (a). Inset: high resolution XPS spectra of the Mo3d peak of the $BaMoO_4$ film. (c) Completely coated sample, surface as received. (d) The same sample after cleaning with 4 keV Ar ions. The last three spectra refer to a partially coated sample: (e) as received, (f) after surface cleaning, and (g) after heavy ion sputtering.

Table 2
XPS peak positions of the prepared $BaMoO_4$ films

Peak	Ba3d5/2	O1s	Mo3d5/2	C1s	Comments
a[a]	784.0 (779.8)[b]	534.5 (530.3)	236.5 (232.3)	288.7	Complete coating
b	783.7 (779.6)	534.1 (530.0)	236.3 (232.2)	288.6	Complete coating
c	780.8 (779.9)	530.9 (530.0)	230.3 (229.4)	285.4	Partial coating
	783.9 (779.2)	534.6 (529.9)	236.4 (231.6)	289.2	
d	781.2	531.4	229.5	285.9	Partial coating
	783.2	534.0	233.9		
e	781.0	531.2	228.7	285.5	Partial coating
			233.6		
*	779.0	529–533	232.5		Standard $BaMoO_4$ PHI
**	779.1	530.5	232.8[c]		Standard $BaMoO_4$ NIST
***				284.5	Standard carbon

[a] The letters refer to Fig. 8.
[b] The values in parentheses are corrected by setting the C1s peak at 284.5 eV.
[c] Mo in $CaMoO_4$.

both spectra exhibit the same amplitude, showing that there is less barium in the partially coated sample. The atomic ratio of Ba:Mo estimated from XPS was 45:55 for the partially coated sample, whereas it was 66:34 for the completely coated sample.

The inset of Fig. 8 shows the high resolution XPS spectra of the Mo3d peak, which exhibits some features detected in all peaks. The bottom of the Fig. 8 shows the spectrum of a sample completely coated [Fig. 3(c), treated in 0.01 M $Ba(OH)_2$ for 1 h]. Curve (c) represents the surface as received, and (d) after cleaning it with 4 keV Ar ions. The doublet observed in curve (c) smears-out, leading to the shoulders in curve (d), an effect which is attributed to surface reduction due to the ion beam. The peak energies shown in Table 2 are displaced 4.1–4.2 eV due to charging effects. The corrected values were calculated by referring the energy scale to the carbon signal at 284.5 eV, 779.8 eV for Ba3d5/2, 232.3 eV for Mo3d5/2, and 530.3 eV for O1s, corresponding to the values for $BaMoO_4$ as found in the databases.[30,31] After surface cleaning, no signal from metallic molybdenum was detected, thus confirming that the surface is completely coated.

The Mo3d peak of a sample that appeared partially coated under the SEM [Fig. 3(a)] is shown in Fig. 8: (e) as received, (f) after surface cleaning, and (g) after heavy sputtering. Spectrum (e) exhibits the Mo3d5/2 peak at two positions, as shown in Table 2. After correcting for surface charging, the large peak located at 231.6 eV could be attributed to Mo in a molybdate state and the smaller one, at 229.4 eV, to partially oxidized molybdenum on the uncoated parts of the foil. Notice the large shift due to surface charging associated with the insulating $BaMoO_4$ crystals. After surface cleaning, the peaks shift to lower binding energies, thus the spectrum in (g) can be interpreted as the superposition of the metallic molybdenum after removal of the molybdenum oxide layer and the Mo(VI) of the $BaMoO_4$ layer. There is an overall decrease in the surface charging induced shift, partially attributed to the reducing effect of the ion beam and also partially because the conducting metallic molybdenum is on the surface.

In summary, (a) the completely coated sample exhibits only barium molybdate, whereas (b) the partially coated ones show a superposition of a strongly shifted molybdate due to surface charging at the isolated islands, and the uncoated (eventually oxidized) molybdenum substrate.

4. Conclusions

Highly crystallized $BaMoO_4$ films can be prepared on metallic molybdenum foils by electrochemical activation in dilute $Ba(OH)_2$ solutions. The pH-concentration diagram for the formation of barium molybdate films has been obtained experimentally. Considering the relatively large solubility of the barium molybdate, a corrected formula for the thickness calculation by the weight gain method has been proposed, which corrects the substrate dissolution effect.

The crystallization of $BaMoO_4$ was characterized by three-dimensional nucleation preferentially at the high stress lines associated with the rolling direction of the substrate foil. We believe that the etching pits are concentrated along these lines. Irregular intergrowth easily formed in the film due to the rapid crystal growth. Our observations are consistent with growth through a dissolution–precipitation mechanism where nucleation starts only after the solution is locally saturated with $BaMoO_4$.

The combination of microanalysis and XPS measurements allowed discrimination between the completely coated and the partially coated samples. The former exhibits solely molybdate, while the latter exhibits the superposition of a strongly shifted molybdate spectrum

due to surface charging at the isolated islands and the spectrum of the uncoated molybdenum substrate.

Acknowledgements

Financial support from FONDECYT under contrcts 3970012 and 11980002 is gratefully acknowledged. The analysis facilities were provided by Fundación Andes through grants c-12510 and c-12776. The authors wish to thank Professor M.E. Pilleux, Professor O. Wittke, Dr. J. Lisoni, Dr. T. Hoffmann, and Dr. R.A. Zarate for their helpful discussions. The authors would also like to thank Solvay-Sabed, Italy, for providing the high purity $Ba(OH)_2$, and Dr. T. Vargas for the use of his electrochemical facility.

References

1. Switzer, J. A., Electrochemical synthesis of ceramic films and powders. *Am. Ceram. Soc. Bull.*, 1987, **66**, 1521–1524.
2. Switzer, J. A., Shane, M. J. and Phillips, R. J., Electrodeposited ceramic superlattices. *Science*, 1990, **247**, 444–446.
3. Switzer, J. A., Hung, C. J., Breyfogle, B. E., Shumsky, M. G., Leeeuwen, R. V. and Golden, T. D., Electrodeposited defect chemistry superlattices. *Science*, 1994, **264**, 1573–1576.
4. Tsukada, T., Venigalla, S. and Adair, J. H., Low-temperature electrochemical synthesis of ZrO_2 films on zirconium substrates: deposition of thick amorphous films and in situ crystallization on zirconium anode. *J. Am. Ceram. Soc.*, 1997, **80**(12), 3187–3192.
5. Switzer, J. A., The n-Silicon/Thallium(III) Oxide Heterojunction Photoelectrochemical Solar Cell. *J. Electrochem. Soc.*, 1986, **133**, 722–728.
6. Yoshimura, M., Yoo, S., Hayashi, M. and Ishizawa, N., Preparation of $BaTiO_3$ thin film by hydrothermal electrochemical method. *Jpn. J. Appl. Phys.*, 1989, **28**, L2007–L2009.
7. Bacsa, B., Ravindranathan, P. and Dougherty, J. P., Electrochemical, hydrothermal, and electrochemical-hydrothermal synthesis of barium titanate thin films on titanium substrates. *J. Mater. Res.*, 1992, **7**(2), 423–428.
8. Bendale, P., Venigalla, S., Verink, E. D., Ambrose, J. R. and Adair, J. H., Preparation of barium titanate films at 55 °C by a electrochemical method. *J. Am. Ceram. Soc.*, 1993, **76**(10), 2619–2627.
9. Venigalla, S., Bendale, P. and Adair, J. H., Low-temperature electrochemical synthesis and dielectric characterization of barium titanate films using non-alkali electrolytes. *J. Electrochem. Soc.*, 1995, **142**(6), 2101–2109.
10. Kajiyoshi, K., Hamaji, Y., Tomono, K., Kasanami, T. and Yoshimura, M., Microstructure of strontium titanate thin film grown by the hydrothermal-electrochemical method. *J. Am. Ceram. Soc.*, 1996, **79**(3), 613–619.
11. Yoo, S. E., Yoshimura, M. and Somiya, S., Preparation of $BaTiO_3$ powders by hydrothermal anodic oxidation method. In *MRS International Meeting on Advanced Materials*, Vol. 3. Materials Research Society, Pittsburgh, PA, 1989, p. 157.
12. Cho, W. S. and Yoshimura, M., Structure evolution of highly crystallized $BaWO_4$ film prepared by an electrochemical method at room temperature. *J. Am. Ceram. Soc.*, 1997, **80**(9), 2199–2204.
13. Cho, W. S., Yashima, M., Kakihana, M., Kudo, A., Sakata, T. and Yoshimura, M., Room temperature preparation of the highly-crystallized luminescent $CaWO_4$ film by a electrochemical method. *Appl. Phys. Lett.*, 1995, **66**(9), 1027–1029.
14. Cho, W. S., Yashima, M., Kakihana, M., Kudo, A., Sakata, T. and Yoshimura, M., Room temperature preparation of the crystallized luminescent $Sr_{1-x}Ca_xWO_4$ solid-solution film by a electrochemical method. *Appl. Phys. Lett.*, 1996, **68**(1), 137–139.
15. Cho, W. S., Yashima, M., Kakihana, M., Kudo, A., Sakata, T. and Yoshimura, M., Active electrochemical dissolution of molybdenum and application for room-temperature synthesis of crystallized luminescent calcium molybdate film. *J. Am. Ceram. Soc.*, 1997, **80**(3), 765–769.
16. Cho, W. S. and Yoshimura, M., Structural evolution of crystallized $SrWO_4$ film synthesized by a solution reaction assisted by electrochemical dissolution of tungsten at room-temperature. *Eur. J. Solid State Inorg. Chem.*, 1997, **34**(9), 895–904.
17. Cho, W. S. and Yoshimura, M., Preparation of highly crystallized $BaMoO_4$ film using a solution reaction assisted by electrochemical dissolution of molybdenum. *Solid State Ionics*, 1997, **100**(1–2), 143–147.
18. Cho, W. S. and Yoshimura, M., Room-temperature synthesis of crystallized luminescent $SrMoO_4$ film by active electrochemical dissolution of molybdenum. *Jpn. J. Appl. Phys., Part 2*, 1996, **35**(11B), L1521–L1523.
19. Cho, W. S., Yashima, M., Kakihana, M., Kudo, A., Sakata, T. and Yoshimura, M., Active electrochemical dissolution of molybdenum and application for room-temperature synthesis of crystallized luminescent calcium molybdate film. *J. Am. Ceram. Soc.*, 1997, **80**, 765–769.
20. Bragg, S. L. and Claringbull, G. F., *Crystal Structures of Minerals (The Crystalline State, Vol. IV)*. G. Belland & Sons Ltd., London, 1965.
21. Lejus, A. M. and Collongues, R., Lanthanide oxides, structural anisotropy, physical and mechanical properties. In *Current Topics in Materials Science, Vol. 4*, ed. E. Kaldis. North-Holland Publishing Co., Amsterdam, 1980, pp. 481.
22. Fuenzalida, V. M. and Pilleux, M. E., Hydrothermally grown $BaZrO_3$ films on zirconium metal: microstructure, X-ray photoelectron spectroscopy, and auger electron spectroscopy depth profiling. *J. Mater. Res.*, 1995, **10**(11), 2749–2754.
23. Weast, R. C., Lide, D. R., Astle, M. J. and Beyer, W. H. (Eds.), *Handbook of Chemistry and Physics*, 70th edn. CRC Press, Boca Raton, FL, 1989, B-75.
24. Lisoni, J. G., Growth Kinetics of $BaTiO_3$ and $BaZrO_3$ Films on TiO_2 and ZrO_2 Single Crystals Under Hydrothermal Conditions, PhD Thesis, Universidad de Chile, Santiago, Chile, 1997 (in Spanish).
25. Follner, H., Clausthal University of Technology, private communication, 1998.
26. PDF-2 Database, Powder Diffraction File, No. 42–1120. International Center for Diffraction Data, Pennsylvania, 1997.
27. Holland, T. J. B. and Redfern, S. A. T., Unit cell refinement from powder diffraction data: the use of regression diagnostics. *Mineral. Mag.*, 1997, **61**, 65–77.
28. Holland, T. J. B. and Redfern, S. A. T., UNITCELL: a nonlinear least-squares program for cell-parameter refinement implementing regression and deletion diagnostics. *J. Appl. Crystallogr.*, 1997, **30**, 84.
29. PDF-2 Database, Powder Diffraction File, No. 29–193. International Center for Diffraction Data, Pennsylvania, 1997.
30. NIST X-Ray Photoelectron Spectroscopy Database v 2.0. US Department of Commerce, Gaithersburg, MD 20899, 1997.
31. Chastain, J., ed., *Handbook of X-Ray Photoelectron Spectroscopy*. Physical Electronics, Eden Prairie, MN, 1992.